ISSN 8756-6990, Optoelectronics, Instrumentation and Data Processing, 2016, Vol. 52, No. 3, pp. 245–251. © Allerton Press, Inc., 2016.
Original Russian Text © A.V. Dmitriev, T.N. Chimitdorzhiev, P.N. Dagurov , 2016, published in Avtometriya, 2016, Vol. 52, No. 3, pp. 37–44.

ANALYSIS AND SYNTHESIS OF SIGNALS AND IMAGES

New Type of Polarization Signature for Radar Images of the Earth Cover with Fractal Properties

A. V. Dmitriev, T. N. Chimitdorzhiev, and P. N. Dagurov

Institute of Physical Material Science, Siberian Branch, Russian Academy of Sciences, ul. Sakh'yanovoi 6, Ulan-Ude, 670047 Russia
E-mail: scidir@ipms.bscnet.ru

Received November 24, 2015

Abstract—A new type of the polarization signature is proposed for estimating the anisotropy of spatial inhomogeneities of the Earth cover with the use of polarimetric radar images taken from space. The case of radar imaging of a pine forest in a decimeter band of wavelengths at different azimuthal angles is considered.

Keywords: remote sensing, synthetic aperture radars, fractal dimension, image processing.

DOI: 10.3103/S8756699016030055

INTRODUCTION

Along with sensors of visible and infrared ranges [1, 2], remote sensing of the Earth (RSE) involves synthetic aperture radars (SARs) [3, 4]. The advantage of radar sensing is imaging process independence of the light conditions of the photographed surface and the presence of clouds. Moreover, radiowaves can penetrate into the underlying surface layers, such as soil, vegetation, snow, and ice, thus, ensuring subsurface sensing. Numerous applications of space-based synthetic aperture radars for mapping of the Earth surface are also due to their high resolution, which is comparable with the resolution of optical systems; for instance, the surface resolution of COSMO-SkyMed and TerraSAR-X radars reaches 1 m. There are many publications on satellite-based radar methods and RSE technologies. Examples of SAR applications can be found in [5], in specialized reviews on biomass estimation [6], in cryospheric studies [7], and in archaeologic research [8].

Specific features of radiowave interaction with complex surface structures that induce multiple scattering or have spatial anisotropy can be found by means of polarization measurements. Such measurements are ensured by a polarimetric SAR radiating linearly polarized waves with vertical (V) and horizontal (H) polarizations and receiving the reflected signal at matched (VV and HH signals) and orthogonal (VH and HV) polarizations. The multichannel mode of radar operation appreciably increases the amount of information extracted from measurements [9, 10].

Wave scattering on complex objects leads to transformations of their polarization. Polarimetric imaging allows one to register the full matrix of scattering for each object and to calculate the elements of this matrix in a certain polarization basis. This fact gave rise to the development of new methods for analyzing RSE data, in particular, methods of scattering matrix decomposition [9, 10] and their modifications. Polarimetric interferometry is used as the basic principle of recently developed methods of the "random volume above the ground" [11–13] and tomography [14, 15] for studying the vertical and volume structure of ground-based objects, in particular, forest.

The above-noted transformations make it possible to obtain polarization "portraits" of the detected objects and to find the physical mechanisms of backscattering, which allows reliable interpretation of RSE data. One of the known methods of polarization analysis is the graphical representation of the radar backscattering coefficient for all possible states of the polarization ellipse, which is obtained in the form of the polarization signature [16]. The latter is a three-dimensional graphical image of polarimetric information about radar

backscattering (brightness of polarimetric radar images): independent variables (the ellipticity and orientation angles of the polarization ellipse) are plotted over the abscissa and ordinate axes, and the echoed radar signal intensity is used as the z axis.

The signatures are constructed for the case with coinciding polarizations of radiation and receiving of the echoed signal (co-polarization signature). A cross-polarization signature is also considered, where the echoed signal is received at an angle perpendicular to the angle of polarization ellipse orientation during radiation. However, this approach cannot adequately capture complex phenomena involved into wave scattering and secondary reflection in inhomogeneous media because the degree of inhomogeneity is not taken into account. Such phenomena can be described by analyzing the texture of the original image. De Grandi et al. [17] studied polarimetric radar images (RIs) by considering a polarization texture signature that implied estimation of spatial fluctuations of radar backscattering, i.e., variations of brightness of image pixels. The variations were estimated on the basis of calculating the normalized second moment reflecting the spatial fluctuations of the echoed radar signal. These fluctuations are affected by speckle noise and spatial variations of radar backscattering (pixel brightness) on inhomogeneities of the scattering volume. However, such a signature does not allow one to estimate the anisotropy of radar backscattering.

The main goal of the present study is to analyze spatial variations of brightness of RI pixels due to anisotropy of inhomogeneous natural media. A new type of the polarization signature is proposed for detection of anisotropy; construction of such a signature is based on studying the fractal characteristics of the polarization response of the medium subjected to remote sensing. The fractal approach was used in the case of linear polarization for analyzing an inhomogeneous natural medium in the form of a forest [18, 19].

In this paper, the approach is extended to various azimuthal angles of radar sensing and arbitrary states of the polarization ellipse, which allows us to refine the estimates of the biophysical parameters of the forest.

CONSTRUCTION OF THE FRACTAL POLARIZATION SIGNATURE

The main idea of the proposed method is the use of the fractal analysis of images in constructing the polarization signature. Estimation of the fractal dimension (FD) is the main method of the quantitative description of fractal properties of examined objects. An available mathematical model representing natural fractal objects is the model of fractional Brownian motion (FBM) [20]. To apply the FBM model to the original RI, the latter is considered as a surface in a three-dimensional space where x and y are the pixel coordinates in the image plane, and the third (z) coordinate is the value of the echoed radar signal. The surface $I(x, y)$ in the FBM model is described by the formula

$$E(|I(x_2, y_2) - I(x_1, y_1)|) \propto \left(\sqrt{(x_2 - x_1)^2 + (y_2 - y_1)^2}\right)^H, \tag{1}$$

where $E(\cdot)$ is the averaging operation, and H is the Hurst exponent ($0 < H < 1$). This surface has the following basic properties:

(a) it is continuous, but not differentiable; all its properties depend on only one scaling coefficient H;

(b) it has a fractal dimension $D = 3 - H$;

(c) it is self-affine.

Equation (1) can be rewritten as

$$E(\Delta I_{\Delta r}) = K \Delta r^H,$$

where $\Delta I_{\Delta r} = |I(x_2, y_2) - I(x_1, y_1)|$, $\Delta r = \sqrt{(x_2 - x_1)^2 + (y_2 - y_1)^2}$, and K is a constant. Taking the logarithm of both sides of the last equation, we obtain

$$\log(E(\Delta I_{\Delta r})) = H \log(\Delta r) + K. \tag{2}$$

Formula (2) is used to estimate the fractal dimensions of images in the following way. First, the values of $E(\Delta I_{\Delta r})$ are calculated for different values of Δr. Then the dependence of $\log(E(\Delta I_{\Delta r}))$ on $\log(\Delta r)$ is plotted. After that, linear regression is applied to determine the slope of the resultant curve, which is equal to H. Knowing H, one can calculate the fractal dimension $D = 3 - H$.

This methods ensures FD estimation for the entire considered surface (entire RI). However, the most interesting aspect is usually the local FD characterizing local variations of the echoed radar signal in a certain vicinity of a chosen point in the original image. It is calculated by the above-described algorithm,

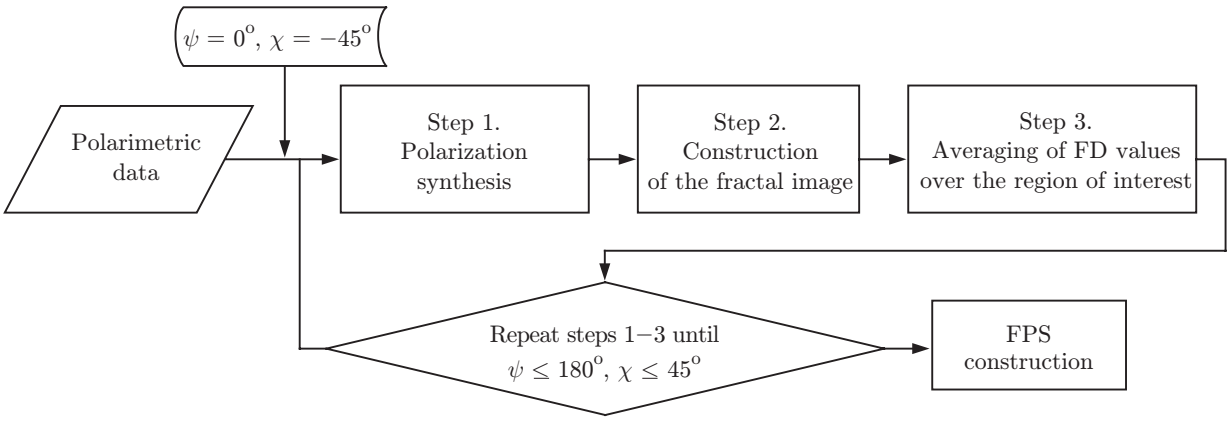

Fig. 1. Flowchart of constructing the fractal polarization signature.

Data of polarimetric radars

SIR-C	ALOS PALSAR-1 (ascending orbit)	ALOS PALSAR-1 (descending orbit)
09.10.1994	28.06.2006	30.05.2006
10.10.1994	13.08.2006	15.07.2006
—	28.09.2006	30.08.2006
—	13.11.2006	15.10.2006
—	31.03.2007	—
—	16.05.2007	—
—	16.11.2007	—
—	02.04.2008	—
—	05.04.2009	—

where the chosen vicinity is considered as an image. Thus, estimating the local FD at each point of the original RI, one can obtain a corresponding fractal image. The software for generation of fractal images was described in [21].

The flowchart of the algorithm for constructing the fractal polarization signature (FPS) is shown in Fig. 1. At the first step, the ranges of variation of the orientation angle ψ ($0 \le \psi \le 180^{\circ}$) and ellipticity angle χ ($-45 \le \chi \le 45^{\circ}$) of the polarization ellipse are divided into uniform sequences of the values of $\{\psi_i\}_{i=0}^{N}$ and $\{\chi_j\}_{j=0}^{M}$. For each combination (ψ_i, χ_j), a co-polarized or cross-polarized image is synthesized in accordance with Eq. (13) from [16]. After that, the synthesized images are transformed to fractal images [21]. A region (or a vicinity of a certain point) for which the signature has to be constructed is defined in these images. The calculated FDs in the chosen region are averaged for obtaining the resultant FD. Thus, one value of D_{ij} is obtained for each pair of the angles (ψ_i, χ_j). The resultant set of $L = (N+1)(M+1)$ points (ψ_i, χ_j, D_{ij}) forms the FPS, which characterizes the spatial fluctuations of radar backscattering.

It should be noted that FPS construction is computationally expensive. The reason is that estimation of the value of one pixel of the fractal image requires processing of $s \times s$ pixels of the original image, where $s = 2r + 1$ (r is the radius of the chosen vicinity). Thus, the number of computations for determining only one FD value increases in proportion to the squared radius of the chosen vicinity. Another factor affecting the computation time is the choice of the step of variation of the polarization ellipse angles. Let δ be the step of the sequences of variation of the polarization ellipse angles. Then we have $N = [180^{\circ}/\delta]$ and $M = [90^{\circ}/\delta]$. For $\delta = 3^{\circ}$, we obtain $N = 60$ and $M = 30$. For FPS construction, it is necessary to synthesize $L = 1891$ polarimetric images and to transform each image to a fractal image. Depending on the original RI size, it takes several hours on a modern personal computer (64-bit computer with an Intel® Core™ i5-4570@3.2 GHz processor). For a step of 1°, it is necessary to process $L = 16471$ images, which substantially increases the computation time.

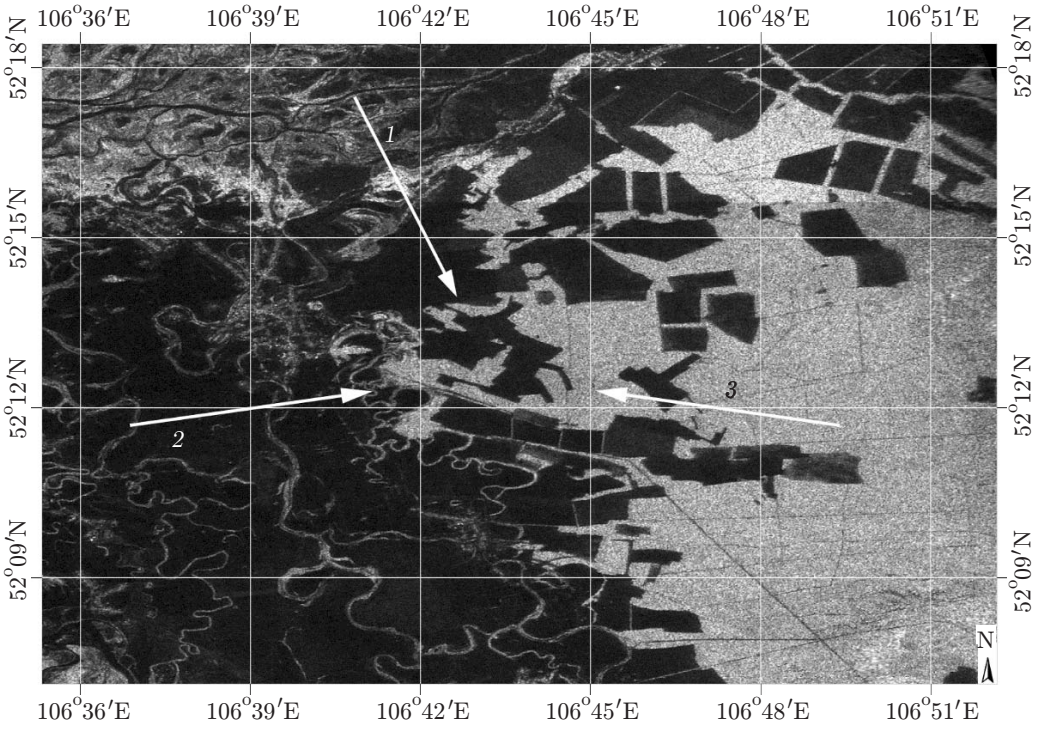

Fig. 2. Radar sensing geometry.

INITIAL DATA, RESULTS, AND DISCUSSION

For constructing the signatures, we used the data of space-based polarimetric SARs: SIR-C, which performed imaging in October 1994, and ALOS, which performed imaging in 2006–2009 (see the table).

Images taken by SIR-C were obtained simultaneously in two ranges (L- and C-bands with wavelengths of 24 and 5.6 cm, respectively) on the ascending orbit with an orbit orientation angle of 62.6° and wave incidence angle of 23.9°; remote sensing was performed in the south-south-east direction (Fig. 2, arrow 1). The orbit orientation angle of ALOS PALSAR-1 was 98.1°, and the incidence angle was 24°; the sensing was performed in the close-to-east direction on the ascending orbit (arrow 2) and in the west direction on the descending orbit (arrow 3). Multilocking was performed for the initial data in order to eliminate the speckle noise. As a result, the pixel size in the images was 24×24 m. The polygon for testing the developed method was a 1×1 km region of a predominantly pine forest on the plain part of the Selenga river estuary. Forest taxation was performed in several chosen regions of the pine forest; the azimuthal distributions of the tree branch directions and the angular distribution in the vertical plane were measured. The results of these measurements showed that the greatest density of branches of 60–75% of trees was observed in the range of azimuthal angles from south-east to south-west. This fact is illustrated by Fig. 3, which shows a photograph of a tree with the above-described distribution of branches. The image obtained by means of imaging in the direction from west to east corresponds to the case of radar sensing indicated by arrow *2* in Fig. 2. The slope of the tree branches varies approximately in the range of angles from 0 to 80° with respect to the horizontal line; the values 0 and 80° refer to the lower and upper branches, respectively. In the middle part of trees, the slope of the branches is mainly around 40–50°. As a whole, the structure of the branch slopes in the vertical plane is versatile and depends on the local density of trees.

Figure 4 shows the classical co-polarization signatures, which characterize the averaged values of radar backscattering, and Fig. 5 shows the fractal co-polarization signatures, which describe spatial variations of radar backscattering.

The abscissa axis in Figs. 4 and 5 shows the angle of orientation of the polarization ellipse, the ordinate axis shows the ellipticity angle, and the applicate axis shows the averaged normalized value of radar backscattering for the classical signature (see Fig. 4) and the fractal dimension for the fractal signature.

Fig. 3. Example of a tree photograph in the test region.

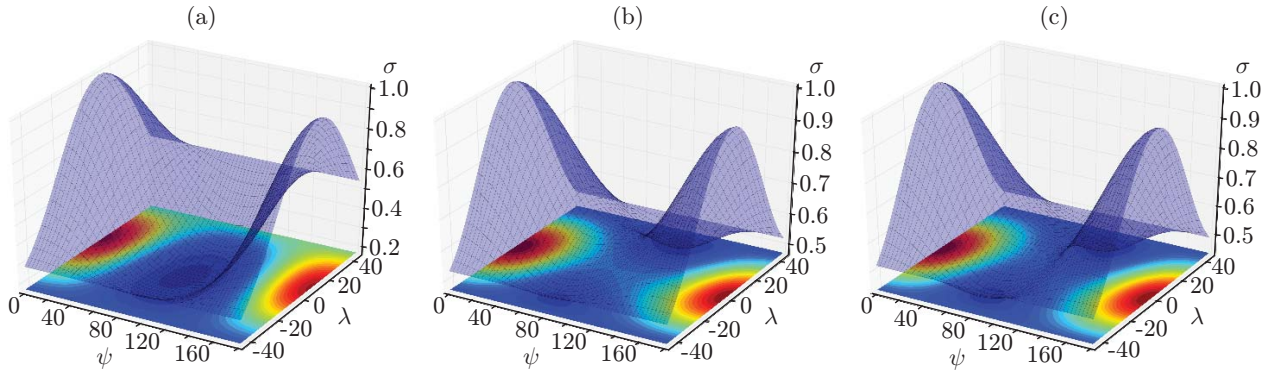

Fig. 4. Polarization signatures (co-polarization): (a) SIR-C; (b) PALSAR (ascending orbit); (c) PALSAR (descending orbit).

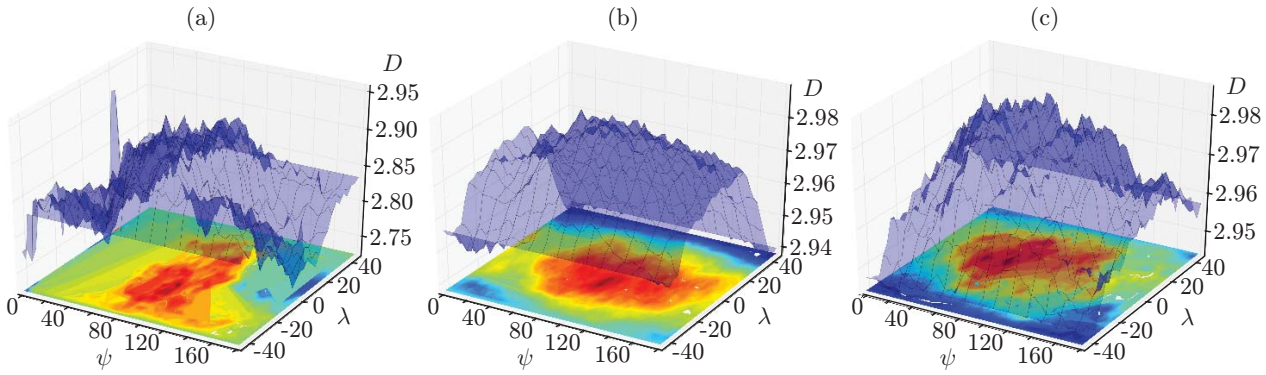

Fig. 5. Fractal polarization signatures (co-polarization): (a) SIR-C; (b) PALSAR (ascending orbit); (c) PALSAR (descending orbit).

The signatures in Fig. 4 are similar in terms of their content and shape, but differ in terms of the pedestal height, which is also a significant characteristic of polarimetric analysis. In this paper, however, the dependence on the pedestal height is not considered.

Let us study the dependence on the polarization orientation angle, assuming that the dependence on the ellipticity angle is symmetric with respect to linear polarization (0° on the ordinate axis). The constructed signature (Fig. 5a) also has a symmetric distribution with respect to the polarization orientation angle of 90°, which is responsible for vertical co-polarization. FD values greater than 2.85 [18] correspond to significant spatial fluctuations of the echoed radar signal. Moreover, these fluctuations correlate with the spatial distribution of inhomogeneities in the form of trunks and large branches [19]. A certain degree of signature symmetry with respect to the ellipse orientation angle of 90° (vertical polarization) is provided by a similar distribution of branches on the western and eastern parts of the trees with remote sensing in the south direction (in the case of SIR-C).

For ALOS PALSAR with remote sensing on the ascending orbit (see Fig. 2), i.e., toward the east, spatial variations of intensity (the FD value is greater than 2.97) are distributed in the range of the polarization ellipse orientation angles of 90–170° (Fig. 5b). For this sensing geometry, where the zero angle of polarization ellipse orientation coincides with the south direction, such an angular distribution testifies that branches on the southern part of the trees form a denser reflecting layer, whereas there are fewer branches on the northern part of the trees, i.e., the spatial distribution of branches is anisotropic.

Conversely, in the case of descending orbits and remote sensing toward the west (so that the zero polarization angle coincides with the north), there is an increasing number of spatial variations observed for orientation angles ranging from20 to 90° (Fig. 5c). This may also be due to a higher density of branches growing toward the south.

For comparative estimates of the fractal analysis results, by analogy with [22], we constructed polarization signatures on the basis of calculating the local Moran's I and Geary's C indices, which actually determine the spatial fluctuations by an autocorrelation method. The above-described effect was observed neither in these signatures, nor in the classical polarization signature [16].

CONCLUSIONS

A new type of the polarization signature is proposed for estimating the structure of spatial fluctuations of the radar backscattering intensity with the use of the fractal analysis, which implies self-similarity at different spatial scales. The physical mechanism of these fluctuations is associated with the influence of speckle noise and spatial variations of radar backscattering owing to inhomogeneity of scattering objects. The fractal signature considered in this paper allows one to estimate anisotropy of the spatial distribution of discrete inhomogeneities, in particular, tree branches. Based on the analysis of signatures obtained by remote sensing of a pine forest, an azimuthal dependence of the distribution of the radar backscattering intensity is obtained, which correlates with the results of the field study of the distribution of branches.

This work was supported by the Federal Agency of Scientific Organizations and by the Russian Foundation for Basic Research (Grant No. 16-08-00646 A).

REFERENCES

1. R. A. Schowengerdt, *Remote Sensing: Models and Methods for Image Processing* (Elsevier, Amsterdam, 2007).
2. S. M. Borzov, A. O. Potaturkin, and O. I. Potaturkin, "Change Detection in Build-Up Areas on the Basis of Structural Features of Satellite Images," Avtometriya **51** (4), 3–11 (2015) [Optoelectron., Instrum. Data Process. 51 (4), 321–328 (2015)].
3. A. I. Zakharov, O. I. Yakovlev, and V. M. Smirnov, *Satellite-Based Monitoring of the Earth: Radar Sensing of the Earth Surface* (Librokom, Moscow, 2012).
4. J. A. Richards, *Remote Sensing with Imaging Radar* (Springer-Verlag, Berlin — Heidelberg, 2009).
5. K. Ouchi, "Recent Trend and Advance of Synthetic Aperture Radar with Selected Topics," Remote Sensing **5** (2), 716–807 (2013).
6. S. Sinha, C. Jeganathan, L. K. Sharma, and M. S. Nathawat, "A Review of Radar Remote Sensing for Biomass Estimation," Intern. J. Environmental Sci. Technol. **12** (5), 1779–1792 (2015).
7. S. D. Jawak, T. G. Bidawe, and A. J. Luis, "A Review on Applications of Imaging Synthetic Aperture Radar with a Special Focus on Cryospheric Studies," Adv. Remote Sensing **4** (2), 163–175 (2015).

8. F. Chen, R. Lasaponara, and N. Masini, "An Overview of Satellite Synthetic Aperture Radar Remote Sensing in Archaeology: From Site Detection to Monitoring," J. Cultural Heritage (2015). http://www.sciencedirect.com/science/article/pii/S129620741500093X.
9. S. R. Cloude, *Polarisation: Applications in Remote Sensing* (Oxford University Press, New York, 2009).
10. J.-S. Lee and E. Pottier, *Polarimetric Radar Imaging: From Basics to Applications* (CRC Press, Boca Raton, 2009).
11. R. N. Treuhaft and P. R. Siqueira, "Vertical Structure of Vegetated Land Surfaces from Interferometric and Polarimetric Radar," Radio Sci. **35** (1), 141–177 (2000).
12. K. P. Papathanassiou and S. R. Cloude, "Single-Baseline Polarimetric SAR Interferometry," IEEE Trans. Geosci. Remote Sensing **39** (11), 2352–2363 (2001).
13. M. Neumann, L. Ferro-Famil, and A. Reigber, "Estimation of Forest Structure, Ground, and Canopy Layer Characteristics from Multibaseline Polarimetric Interferometric SAR Data," IEEE Trans. Geosci. Remote Sensing **48** (3), 1086–1104 (2010).
14. A. Reigber and A. Moreira, "First Demonstration of Airborne SAR Tomography Using Multibaseline L-Band Data," IEEE Trans. Geosci. Remote Sensing **38** (5), 2142–2152 (2000).
15. S. Tebaldini, "Single and Multipolarimetric SAR Tomography of Forested Areas: A Parametric Approach," IEEE Trans. Geosci. Remote Sensing **48** (5), 2375–2387 (2010).
16. J. J. Van Zyl, H. A. Zebker, and C. Elachi, "Imaging Radar Polarization Signatures: Theory and Observation," Radio Sci. **22** (4), 529–543 (1987).
17. G. De Grandi, J.-S. Lee, D. Schuler, and E. Nezry, "Texture and Speckle Statistics in Polarimetric SAR Synthesized Images," IEEE Trans. Geosci. Remote Sensing **41** (9), 2070–2088 (2003).
18. T. N. Chimitdorzhiev, V. E. Arkhincheev, A. V. Dmitriev, and B. Z. Tsyplakov, "Fractal Analysis of Radar Polarimetric Data for Classification of the Earth Cover," Issled. Zemli iz Kosmosa, No. 4, 27–33 (2007).
19. T. N. Chimitdorzhiev, V. E. Arkhincheev, and A. V. Dmitriev, "Polarimetric Estimation of Spatial Fluctuations of Radar Images for reconstructing the Structure of the Forest Canopy," Issled. Zemli iz Kosmosa, No. 5, 80–82 (2007).
20. B. B. Mandelbrot and J. W. van Ness, "Fractional Brownian Motions, Fractional Noises and Applications," SIAM Rev. **10** (4), 422–437 (1968).
21. N. Tustison and J. Gee, "Stochastic Fractal Dimension Image," The Insight J. (2009). http://hdl.handle.net/1926/1525.
22. S. W. Myint, "Fractal Approaches in Texture Analysis and Classification of Remotely Sensed Data: Comparisons with Spatial Autocorrelation Techniques and Simple Descriptive Statistics," Intern. J. Remote Sensing **24** (9), 1925–1947 (2003).